Skin Aging in Long-Lived Naked Mole-Rats is Accompanied by Increased Expression of Longevity-Associated and Tumor Suppressor Genes

Iqra Fatima [1], Guodong Chen [8], Natalia V. Botchkareva [8], Andrey A. Sharov [8],

Daniel Thornton [2], Holly N. Wilkinson [3], Matthew J. Hardman [3], Andreas Grutzkau [4],

Joao Pedro de Magalhaes [2], Andrei Seluanov [5], Ewan St. J. Smith [6], Vera Gorbunova [5],

Andrei N. Mardaryev [1]*, Chris G. Faulkes [7]*, Vladimir A. Botchkarev [8]*

[1] Centre for Skin Sciences, Faculty of Life Sciences, University of Bradford, UK

[2] Integrative Genomics of Ageing Group, Institute of Integrative Biology, University of Liverpool, UK

[3] Centre for Atherothrombosis & Metabolic Disease, Hull York Medical School, University of Hull, UK

[4] Deutsches Rheuma-Forschungszentrum Berlin, an Institute of the Leibniz Association, Germany

[5] Departments of Biology and Medicine, University of Rochester, NY, USA

[6] Department of Pharmacology, University of Cambridge, UK

[7] School of Biological and Chemical Sciences, Queen Mary University of London, UK

[8] Department of Dermatology, Boston University School of Medicine, MA, USA

*Corresponding and communicating author:

*Dr. Vladimir Botchkarev, Department of Dermatology, Boston University School of Medicine, 609 Albany Street, Boston, MA 02118, USA; Email: vladbotc@bu.edu

*Equal contribution as corresponding authors

Short title: Skin aging in long-lived naked mole rats

Abstract

Naked mole rats (NMRs, *Heterocephalus glaber*) are long-lived mammals that possess a natural resistance to cancer and other age-related pathologies, maintaining a healthy life span for >30 years. Here, using immunohistochemical and RNAseq analyses, we compare skin morphology, cellular composition and global transcriptome signatures between young and aged (3-4 versus 19-23-year-old) NMRs. We demonstrate that similar to human skin, aging in NMRs is accompanied by a decrease of epidermal thickness, keratinocyte proliferation, and a decline in the number of Merkel cells, T-cells, antigen-presenting cells and melanocytes. Similar to human skin aging, expression levels of dermal collagens are decreased, while Mmp-9 and Mmp-11 levels increased in aged versus young NMR skin. RNAseq analyses reveal that in contrast to human or mouse skin aging, the transcript levels of several longevity-associated (*Igfbp3, Igf2bp3, Ing2*) and tumor-suppressor genes (*Btg2, Cdkn1a, Cdkn2c, Dnmt3a, Hic1, Socs3, Sfrp1, Sfrp5, Thbs1, Tsc1, Zfp36*) are increased in aged NMR skin. Overall, these data suggest that specific features in the NMR skin aging transcriptome might contribute to the resistance of NMRs to spontaneous skin carcinogenesis and provide a platform for further investigations of NMRs as a model organism for studying the biology and disease resistance of human skin.

Introduction

The skin forms an interface between the external environment and internal milieu that protects mammalian organisms against uncontrolled water loss and numerous environmental stressors, including mechanical injury, UV irradiation, thermal/chemical insults, harmful microorganisms and viruses (Chuong et al., 2002, Larsen et al., 2020, Menon and Kligman, 2009, Slominski et al., 2012). To fulfil such complex functions, different cell lineages of epithelial, mesenchymal and neuro-ectodermal origin interact with each other and form a robust and plastic biological system capable of maintaining homeostasis and responding efficiently to environmental challenges (Rognoni and Watt, 2018).

Similar to other organs, the skin undergoes both intrinsic (chronological) and extrinsic (environmental) aging associated with changes in visual appearance and loss of functional capacity and regenerative potentials (Rittie and Fisher, 2015, Yaar et al., 2002). Major age-related changes in the skin include wrinkling, dryness, pigmentation abnormalities and the development of a variety of benign neoplasms (Yaar et al., 2002). Microscopically, skin aging is accompanied by the decrease of epidermal thickness and keratinocyte proliferation, decline in the number of melanocytes and Langerhans cells, flattening of the dermal-epidermal junction, decline of dermal volume and cellularity, fragmentation of collagen and elastic fibers, decrease of dermal blood/lymphatic vessels, cutaneous innervation and sensory perception (Rittie and Fisher, 2015, Yaar et al., 2002).

At the molecular level, aging of the epidermis is accompanied by alterations of gene expression in the keratinocyte-specific gene loci, loss of terminal differentiation-associated calcium gradient, decreased lipid synthesis and hyaluronic acid content, cytokine imbalance, and results in compromised epidermal barrier function (He et al., 2020). Thinning and flattening of the

dermal-epidermal junction in aged skin is accompanied by a significant reduction in the levels and distribution of collagens IV/VII/XVII, integrin β4, and laminin-332 (Langton et al., 2016). Dermal changes in aged skin also include fragmentation of both collagen and elastic fibers, a decrease in the levels of major extracellular matrix components (decorin, versican), and upregulation of the matrix metallopeptidases (MMP1/3/9) that cleave collagen and elastic fibrils (Cole et al., 2018).

Age-associated alterations in the skin immune system include a decrease in the antigen-presenting and migratory capacities of Langerhans and dendritic cells, resulting in alterations of the barrier immunity and development of chronic low-grade inflammation (inflammaging) (Pilkington et al., 2021). Accumulation of senescent cells in the aged epidermis and dermis (Gunin et al., 2014, Victorelli et al., 2019, Waaijer et al., 2016) contributes to the "inflammaging" phenotype due to their production of pro-inflammatory cytokines as a part of Senescent-Associated Secretory Phenotype (SASP) (Toutfaire et al., 2017).

There are quite legitimate concerns among many researchers raising the question of whether mechanisms of aging identified in short-lived mammals, such as mice or rats, adequately reflect the complexity of longevity pathways that regulate aging in long-lived species like humans (Dammann, 2017). Naked mole rats (NMRs, *Heterocephalus glaber*) are long-lived rodents possessing remarkable resistance to spontaneous carcinogenesis, certain noxious stimuli and hypoxia and maintain sustained healthy life-span span for over 30 years (Buffenstein, 2005, Gorbunova et al., 2014, Seluanov et al., 2018, Smith et al., 2020). Comparative genome analyses have revealed that the NMR genome shows higher similarity (93% synteny) to the human genome compared to that of mice (83%) or rats (80%) (Gladyshev et al., 2011, Kim et al., 2011). Many aspects of the NMR biology have recently been extensively discussed (Braude et al., 2021, Buffenstein et al., 2021) leading to the conclusion that exceptional resistance of NMRs to aging-

associated pathologies is mediated by several mechanisms, including more robust DNA repair and genome stability compared to mice, a unique organization of the tumor suppressor *Ink4a/b* locus, production of large amounts of higher molecular weight hyaluronic acid with unusual properties, altered IGF receptor signaling and increased proteasome activity and protein stability (Brohus et al., 2015, Del Marmol et al., 2021, Evdokimov et al., 2018, Gorbunova et al., 2014, Keyes et al., 2013, Kulaberoglu et al., 2019, MacRae et al., 2015, Rodriguez et al., 2016, Seluanov et al., 2018, Takasugi et al., 2020).

The skin of the NMR displays distinctive morphological features associated with adaptation of these animals to the subterranean environment: relatively thick epidermis with unusually thick corneal layer, presence of pigment-containing cells in the dermis, lack of hair follicles on most of the skin (Daly and Buffenstein, 1998, Menon et al., 2019, Thigpen, 1940). However, it is unclear how the NMR skin changes during aging and whether there are any particular features in the NMR skin transcriptome that underlie the remarkable natural resistance of NMRs to spontaneous skin carcinogenesis.

In this manuscript, we show that skin aging in the NMR resembles many features of human skin aging, including histological and biochemical changes in both the epidermis and dermis. However, in contrast to human skin, transcripts and proteins of several longevity-associated and tumor suppressor genes are increased in the NMR skin during aging. These data suggest that these features of the NMR skin aging transcriptome might contribute to the resistance of NMRs to spontaneous skin carcinogenesis, thus reaffirming the potential of the NMR as a model organism for studying both the biology and disease of human skin.

Results

Epidermis of aged NMRs shows decreased thickness, cell proliferation and reduced expression of the keratinocyte differentiation markers, Col17a1 and Merkel cells

To assess the impact of aging on NMR skin, we first compared visual appearance, morphological parameters and expression of established keratinocyte differentiation markers between the dorsal skin epidermis of young (2-4.5 year-old) and aged (19-23-year-old) animals (**Fig. 1 A**). Consistent with data published previously (Daly and Buffenstein, 1998, Tucker, 1981), the dorsal skin of NMRs has a wrinkled and saggy macroscopic appearance, and a lack of any skin appendages (**Fig. 1 B**). Single unpigmented hairs are only visible at the lateral part of the body, while vibrissa hairs are numerous at the facial skin (**Fig. 1 A**). In contrast to the skin of young NMRs (YNMRs), the skin of old NMRs (ONMRs) appeared thinner, more translucent and less pigmented (**Fig. 1 B**). Histologically, the dorsal skin of YNMRs presented a relatively thick multi-layered epidermis with a thick stratum corneum (Menon et al., 2019), while in ONMRs, the epidermal thickness was significantly reduced (**Fig. 1 C**). The majority of Ki67+ cells were located in the basal epidermal layer, while their number was markedly decreased in ONMRs versus YNMRs (**Fig. 1 D**).

In the NMR epidermis, Krt14 expression was mainly confined to the basal layer, while Krt10 and Loricrin (Lor) were seen in the spinous and granular layers, respectively (**Fig. 1 E-G**). However, the immunofluorescence intensity for all three markers, as well as for p63 transcription factor, a master regulator of epidermal development and differentiation (Koster et al., 2007), was significantly decreased in the epidermis of ONMRs compared to YNMRs (**Fig. 1 E-H**).

The expression of Col17a1, an established marker of epidermal aging (Liu et al., 2019), was also decreased in basal epidermal keratinocytes and dermal-epidermal basement membrane

of ONMRs, compared to YNMRs (**Fig. 1 I**). In addition, the number of Krt20+ Merkel cells, specialized sensory cells involved in mechanotransduction (Jenkins et al., 2019), was significantly lower in the epidermis of ONMRs versus YNMRs (**Fig. 1 J**). However, epidermal Caspase 3+ apoptotic cells did not reveal any differences in their number between YNMRs and ONMRs (**Figure S1 A**).

Age-associated changes in the NMR dermis include decreased Col1a1 expression, an increase in Mmp9 and Mmp11, and loss of melanocytes

The NMR epidermis forms invaginations or buds elongating into the dermis (Tucker, 1981). Their numbers was significantly decreased in ONMRs contributing to age-associated flattening of the epidermal-dermal interface (**Fig. 2 A**). Similar to human skin (Langton et al., 2010), Fibrillin-2-enriched elastic fibers in the papillary dermis of NMRs formed candelabra-like cascades ascending towards the dermal-epidermal junction and epidermal buds, while their number were not changed between YNMRs and ONMRs (**Fig. 2 B**). Moreover, the distribution of dermal elastic fibers and Elastin expression levels were quite similar in the dermis of YNMRs and ONMRs (**Figure S1 B**).

Col1a1, an important component of the mature collagen fibers providing tensile strength to the skin (Cole et al., 2018), was broadly expressed in the papillary and reticular dermis of YNMRs (**Fig. 2 C**). In ONMRs, dermal Col1a1 expression declined compared to YNMRs (**Fig. 2 C**), while expression levels of Col3a1, a marker of immature collagen fibers, did not show significant differences between YNMRs and ONMRs (**Figure S1 C**).

Matrix metalloproteinases (Mmps) promote age-associated extracellular matrix remodeling (Cole et al., 2018). Immunohistochemical revealed a marked increase of Mmp9 and

Mmp11 immunofluorescence in the dermis of ONMRs compared to YNMRs (**Fig. 2 D, Figure S1 E**). However, Mmp1 levels did not show significant changes in ONMRs versus YNMRs (**Figure S1 D**).

The NMR extracellular matrix contains hyaluronic acid (HA), which unlike mouse HA forms highly folded structures that may contribute to the elasticity of NMR skin (Kulaberoglu et al., 2019). Moreover, HA appears to be present in larger amounts and has a higher molecular weight in NMR than mouse or guinea pig (Del Marmol et al., 2021, Keyes et al., 2013). However, Hyaluronan-Binding Protein (HABP) immunostaining used previously for analyses of the HA content in the skin (Kulaberoglu et al., 2019) and the HA receptor Cd44 levels did not show any differences between the dermis of YNMRs and ONMRs (**Fig. 2 E, F**).

One of the characteristic features of the NMR dorsal skin is the presence of a large number of pigmented melanocytes in the dermis (Daly and Buffenstein, 1998). Consistently with the visual loss of skin pigmentation in old NMRs (**Fig. 1 A**), Warthin-Starry staining of melanin (Joly-Tonetti et al., 2016) revealed a dramatic decrease of the areas covered by pigment in the dermis of ONMRs compared to YNMRs (**Fig. 2 G**). Also, the number of melanocytes expressing gp100 that is expressed in melanogenically active melanocytes (Watt et al., 2013), was markedly reduced in the dermis of ONMRs (**Fig. 2 H**).

Aged NMR skin exhibits decreased Cd3ε T-cells, MHC class II antigen-presenting cells, mast cells and increase of senescent cells

To characterize changes in the skin immune system occurring during aging in NMRs, we used a panel of primary antibodies established for analysis of immune cell markers in NMRs (Shebzukhov et al., 2019). Comparative studies of the immune cell markers revealed that ONMRs

show a significant decrease in the number of Cd3ε-positive T-cells and MHC II-positive cells in the epidermis and dermis (**Fig. 3 A, B**; **Figure S1 F**). A quantitative analysis of Cd8+cells and Cd11b+ (macrophages) cells in the dermis did not reveal any differences between ONMRs and YNMRs (**Fig. 3 C, Fig. 3 D**). In contrast, the number of mast cells was significantly lower in the dermis/subcutis of old NMRs compared to young animals (**Figure S2 H**).

The presence of senescent cells in the skin of NMRs was previously reported (Zhao et al., 2018). Senescence-associated β-galactosidase (SA-β-gal) staining revealed a significant increase in the number of SA-β-gal-positive cells in the aged epidermis, and only a tendentious increase in the dermis of ONMRs, which did not reach statistical significance (p=0.082, **Fig. 3 E**). The increase in the number of senescent cells in the ONMR skin was accompanied by the elevated expression of $p16^{INK4a}$ transcript as an important marker of senescent cells (Ressler et al., 2006) that was determined by qRT-PCR in full-thickness skin samples (**Figure S1 G**). However, the expression of both $p15^{INK4b}$ and $pALT^{INK4a/b}$ transcripts remained unaltered in old versus young skin (**Figure S1 G**).

Transcriptome analysis of NMR aging skin reveals changes in the expression of extracellular matrix-associated genes, components of the IGF signaling pathway, regulators of glucose metabolism and cell proliferation

To further characterize changes occurring in the NMR skin during aging on the molecular level, RNAseq analyses of the full-thickness skin of 4-year-old and 19-year-old animals were preformed and revealed significant (two-fold and higher) changes in the expression of 768 genes between the skin of YNMRs and ONMRs (**Fig. 4 A, B**). Overall, RNAseq data were concordant with our histomorphology/immunohistochemistry results (**Fig. 1, Fig. 2, Table S3**) and identified

the decline in expression of dermal collagen genes (*Col1a1, Col1a2)*, genes encoding T-cell and Langerhans cell markers (*Thy1, Cd3d, Cd207),* as well as of melanocyte/melanogenesis-associated markers (*Dct, Tyrp1, Slc24a5*) in ONMR skin compared to YNMRs (**Fig. 4 C**, **Tables S2, S3**). Consistent with the immunohistochemistry results (**Fig. 2 D, Figure S1 D**), RNAseq analyses also detected an increase in *Mmp9* and *Mmp11* gene expression in ONMR versus YNMR skin (**Fig. 4 C, Table S1**).

Interestingly, among the group of extracellular matrix-associated genes differentially expressed in the ONMR skin, we found a marked downregulation of numerous collagen genes, including *Col1a1, Col1a3, Col3a1,* genes encoding the enzymes involved in collagen synthesis (*Pcolce, Pcolce2),* and fibrillogenesis (*Cthrc1, Sparc*) (**Fig. 4 A-C, Table S2**). Also, several genes encoding extracellular matrix-degrading enzymes (*Mmp11, Mmp9, Pm20d2, Adamts5*) were upregulated in the skin of ONMRs, while *Mmp27* and *Mmp19* were downregulated compared to YNMRs (**Fig. 4 A-C, Tables S1, S2**). Although it is known that MMP9 and MMP11 can be processed by other MMPs, such as MMP2 (Bonnans et al., 2014), we observed no difference in expression levels of *Mmp2,* as well as of transcript of other enzyme involved in the MMP processing/cleavage *Furin* between ONMR and YNMR skin (data not shown).

A group of genes involved in the regulation of glucose metabolism included *Pdk4*, which encodes pyruvate dehydrogenase kinase 4 promoting a switch from oxidative energy metabolism to glycolysis (Stacpoole, 2012). *Pdk4* was strongly upregulated in the skin of ONMRs, as well as the *Pck1* gene, a critical regulator of gluconeogenesis, *Acacb* encoding a key enzyme in fatty acid synthesis, and *Slc2a6* encoding the glucose transporter Glut6 (Barron et al., 2016).

IGF signaling is implicated in the control of longevity (Brohus et al., 2015) including skin aging (Lewis et al., 2010). RNAseq analysis revealed that expression of *Igf1* was decreased in

ONMR skin compared to YNMRs, while expression levels of transcripts for the IGF-1/2 binding proteins *Igfbp3* and *Igf2bp3* were increased (**Tables S1, S2**).

The group of genes involved in cell cycle regulation that show differences in expression between ONMR and YNMR skin included cyclin-dependent kinase inhibitors (*Cdkn1a, Cdkn2c*) and member of the anti-proliferative BTG/TOB family (*Btg2*), whose expression patterns in aged skin were upregulated (**Fig. 4 C, Table S1**). These changes were accompanied by decreased expression of genes positively regulating cell proliferation including *Pcna, Ccne1* gene encoding cyclin E1, centromere-associated protein genes (*Cenph, Cenpm, Cenpn, Cenpw, Cenpx*), genes controlling mitotic cell division (*Ncapg2, Pole1, Tk1)* and cell cycle-associated transcription machinery (*E2f1*) (**Fig. 4 C, Table S2**). The significant increase of Cdkn1a, Btg2 and Tob1 at the protein level in the NMR aged epidermis were further confirmed by quantitative immunofluorescence analysis (**Figure S3**). These data were consistent with the results demonstrating the decrease of epidermal proliferation in ONMRs compared to YNMRs (**Fig. 1 D**).

Species-specific differences in aging transcriptomes hint to a potential contribution to longevity and cancer resistance in NMRs

To correlate the age-associated changes in the NMR skin transcriptome to human or mouse skin aging, we compared our data with four publicly available RNAseq skin aging datasets obtained from either full-thickness skin or epidermis of human and mouse skin (young versus aged) (Aramillo Irizar et al., 2018, Barth et al., 2019, Ge et al., 2020, Raddatz et al., 2013). This analysis revealed that only a relatively small number of genes whose expression was changed in the ONMR skin (11.7% of upregulated and 16.9% of downregulated genes), showed a similar trajectory in the aged human and mouse skin. Surprisingly, most genes differentially expressed

during NMR skin aging were not changed in either human or mouse skin aging, while small number of differentially expressed genes (11.0% and 14.5% of up- and downregulated genes, respectively) in the NMR aging transcriptome showed opposite dynamics to aged human or mouse skin (**Figure S2, Tables S4, S5**).

To further correlate the relevance of age-associated changes in the NMR cutaneous transcriptome to other age-related datasets, we used the Human Ageing Genome Resource (HAGR) database platform (Tacutu et al., 2018). We found that 113 genes differentially expressed in ONMR skin (16.3% of the upregulated and 12.9% of downregulated genes, defined as NMR aging signature genes) were present in one or more HAGR datasets (**Fig. 5 A; Table S6**). According to the HAGR databases, substantially more NMR aging signature genes were relevant to human aging than to the animal aging (33 versus 12, respectively), while 8 NMR genes belonged to both datasets (GeneAgeHuman, GeneAgeModel; **Table S6**).

In ONMR skin, RNAseq detected elevated expression of *Fos* and *Jun* (**Table S1**), encoding essential components of the AP-1 transcription factor, stimulating the expression of MMPs during UV-induced photoaging in human skin (Rittie and Fisher, 2002, 2015). Also, among the genes upregulated in ONMR skin was *Igfbp3* implicated in the control of longevity and counteracting the life-shortening effects of IGF signaling (Martins et al., 2016), as well as anti-proliferative genes *Cdkn1a* and *Cdkn2c* (**Table S6**). Protein-protein interaction network analysis performed using the STRING software tool (http://string-db.org, vision 11.0) (Crosara et al., 2018) revealed links between the Fos/Jun genes with tumor suppressor genes *Cdkn1a*/*Cdkn2c*/*Zfp36* upregulated in ONMR skin (**Figure S4**). On the other hand, the longevity-related genes downregulated in ONMR skin formed network controlling extracellular matrix remodeling, IGF signaling and DNA replication/cell division (**Figure S5**).

Because NMRs show remarkable resistance to spontaneous carcinogenesis, we intersected the age-associated NMR transcriptome with the human Cancer Gene Census (CGC) database (Welcome Sanger/EBI, Hinxton, UK) (Sondka et al., 2018) and Tumor Suppressor Genes (TSG) database (University of Texas, Houston, TX). We found that 67 differentially expressed genes in the ONMR skin were present in the CGC/TSG databases, representing the NMR cancer-related/TSG signature genes (**Fig. 5 B**). Interestingly that this group of genes contained not only inhibitors of IGF pathway, but also inhibitors of the JAK/STAT (*Sosc3)* and Wnt pathways (*Sfrp1* and *Sfrp5)* (**Table S7**).

After merge of the longevity-associated and cancer-related/TSGs genes, we found 21 common genes seen in the HAGR and CGC/TSG databases (**Fig. 5 C**), thus demonstrating their relevance to both longevity and cancer development/resistance. The group of the longevity/cancer-related/TSG signature genes upregulated in ONMR skin (**Fig. 5 C)** included cell cycle inhibitors *Cdkn1a/Cdkn2c* (Winkler, 2010), tumor suppressor *Hic1* gene encoding transcriptional repressor downregulated in many cancers (Rood and Leprince, 2013), as well as *Tsc1* gene mutated in Tuberous Sclerosis Complex disease characterized by formation of tumor-like lesions (hamartomas) in the skin (Rosset et al., 2017). Also, expression of *Zfp36* gene encoding RNA-binding protein tristetraprolin (TTP) inhibiting formation of squamous cell carcinomas (Assabban et al., 2021) was upregulated in ONMR skin (**Fig. 5 C**). In addition, expression of *Dnmt3a* regulating *de-novo* DNA methylation (Parry et al., 2021) increased in ONMR skin compared to YNMRs (**Table S7**).

Among the longevity-associated/cancer-related genes downregulated in ONMR skin (**Fig. 5 C**) were proto-oncogene *Ret*, transcription factor *E2f1* promoting cell proliferation and upregulated in chemically-induced squamous cell carcinomas (Balasubramanian et al., 1999), and

Tp63 downregulated in human skin during aging (**Fig. 5 C**). Protein-protein interaction network of the cancer-related/TSG genes revealed additional links between a group of tumor suppressors (*Btg2, Sfrp1, Socs3, Thbs1*) and oncogenes (*Abl1, Flt3, Kras, Sparc*), as well as between DNA methyltransferase *Dnmt3a,* components of the FGF signaling pathway *Flt3/Fgfr4* and longevity-related *Tp63* (**Figure S6**).

The comparative analyses of the longevity-associated/cancer-related/TSG signature genes in the NMR aging transcriptome with human or mouse skin aging datasets (Aramillo Irizar et al., 2018, Barth et al., 2019, Ge et al., 2020, Raddatz et al., 2013) revealed that none of the 13 genes of this category upregulated in ONMR skin were significantly elevated in aged human or mouse skin, while expression of only 1 out of 8 genes downregulated in ONMR skin showed similar changes in human or mouse skin (**Fig. 5 C, Tables S6, S7**). These data suggest that age-associated changes in the cancer-related NMR transcriptome show unique features that may underlie the remarkable resistance of NMRs to spontaneous skin carcinogenesis.

Discussion

In this report, we provide evidence that skin aging in NMRs shows many similar features to the aging process in human skin, including: 1) Decrease of epidermal thickness, keratinocyte proliferation and expression of epidermal keratins; 2) Decline in the number of Merkel cells and increase of senescent cells in the epidermis; 3) Flattening of the epidermal/dermal border, decrease in expression levels of dermal collagens and upregulation of Mmp-9 and Mmp-11; 4) Loss of skin pigmentation and decline in the number of dermal melanocytes; 5) Decline in the number of epidermal/dermal T-cells and antigen-presenting cells.

Our data showing morphological and biochemical changes in the skin of 19-23 year-old NMRs appears to be quite different from the data obtained from 11 year-old animals (Savina et al., 2020) and demonstrate that skin aging in NMRs occurs during last trimester of life. Age-associated changes in the NMR epidermis are consistent with decline in the expression of the p63 transcription factor controlling keratinocyte proliferation, differentiation and preventing premature skin aging (Botchkarev and Flores, 2014, Koster et al., 2007, Su et al., 2009). Signaling/transcription factor-regulated and epigenetic mechanisms operate in concert in controlling epidermal differentiation (Ahmed et al., 2014, Botchkarev, 2017, Botchkarev et al., 2012, Fessing et al., 2011, Kouwenhoven et al., 2015, Mardaryev et al., 2016, Qu et al., 2019, Rapisarda et al., 2017). Skin aging in NMRs is accompanied by accumulation of DNA methylation at specific aging-associated differentially methylated CpGs (Horvath et al., 2022, Lowe et al., 2020). In this context, upregulation of genes encoding DNA methyltransferase *Dnmt3a* and methyl-CpG binding protein *Mecp2* (**Table S1**) might contribute to the changes in aging-associated methylome and gene transcription in the skin of ONMRs.

Similarly to human skin (Waaijer et al., 2012, Waaijer et al., 2018), aged NMRs also show an increase in the number of senescent cells associated with the upregulation of *p16*^{INK4a} in the skin. Senescent cells are present in the NMR skin, and NMR dermal fibroblasts are more resistant to induction of stress-induced premature senescence than mouse fibroblasts (Zhao et al., 2018). In aging human skin, senescent cells produce pro-inflammatory cytokines and contribute to cutaneous inflammaging (Pilkington et al., 2021, Toutfaire et al., 2017). However, detailed transcriptome/proteome analyses of the distinct cell lineages (epithelial, mesenchymal, immune/ vascular, pigment, etc.) are required to define the contribution of the senescent cells and their secretory products to the development of age-associated changes in the NMR skin, including cutaneous immune surveillance and inflammatory response.

Despite their remarkable longevity, NMRs also exhibit a potent resistance to spontaneously developing cancers (Seluanov et al., 2018), with a lack of any reported skin cancer incidence, including basal/squamous cell carcinomas and malignant melanomas (Delaney et al., 2013). Our immunohistochemical data showing a lack of decline in the levels of HA and Cd44 receptor in aged NMR skin suggest that cytoprotective and anti-cancer properties of HA (Keyes et al., 2013, Takasugi et al., 2020) are likely not compromised during aging. Comparative transcriptome analyses reveal that in contrast to human or mouse skin, skin aging in NMRs is accompanied by upregulation of several classes of tumor suppressor genes: secreted inhibitors of the IGF, JAK/STAT and Wnt signaling pathways (*Igfbp3, Igf2bp2, Socs3, Sfrp1, Sfrp5)*, cell cycle inhibitors (*Btg2, Cdkn1a, Cdkn2c)*, transcriptional repressor *Hic1*, RNA-binding protein *Zfp36* and epigenetic regulators (*Dnmt3a, Mecp2*). We speculate that together with other longevity-associated genes, these genes form a multi-level regulatory network mediating cancer resistance in the NMR skin.

Undoubtedly, further analyses are required to fully understand the roles of signaling/transcription factor-mediated and epigenetic regulatory mechanisms controlling the age-associated increase in the expression of the longevity-associated and tumor suppressor genes, as well as downregulation of cancer-related genes in the skin of NMRs. Furthermore, age-associated changes in the NMR cutaneous transcriptome need to be correlated with the proteome and protein activity due to post-transcriptional and post-translational modifications (Buccitelli and Selbach, 2020). These analyses will help define the unique features of the NMR skin aging transcriptome that might contribute to the resistance NMRs exhibit to spontaneous skin carcinogenesis.

Identification of these mechanisms and their relevance to human skin aging might be beneficial for developing novel approaches for the management of age-associated skin conditions, including skin cancer in humans. Taken together, these data provide a platform for further exploration of NMRs as an innovative model organism for studying the biology of human skin and serve as the starting point in the identification of novel mechanisms mediating skin resistance to age-associated pathologies in these unique mammals.

Materials and Methods

Animals and tissue collection

All experiments were conducted in accordance with the United Kingdom Animal (Scientific Procedures) Act 1986 Amendment Regulations 2012 under a Project Licenses granted to A.M. (University of Bradford) and to E. St. J. S. (University of Cambridge) by the Home Office. Animals were maintained in a custom-made caging system with conventional mouse/rat cages connected by different lengths of tunnel. The room was warmed to 28 °C, 50-60% humidity levels was maintained, and bedding, nesting material and water-enriched food were provided. Four young adult NMRs (3-4.5 year-old) and three aged NMRs (19-23 year-old) of both sexes were used in this study. Samples were collected from the dorsal skin, covered in Tissue-Tek medium (VWR, UK), snap-frozen in liquid nitrogen, and stored in −80 °C freezer (Botchkarev et al., 1998, Botchkarev et al., 1999).

Histology, histomorphometry and immunohistochemistry

For histology, 10 um cryosections were fixed in 4% PFA followed by haematoxylin/eosin staining, or by Giemsa staining for mast cell visualization, or by the modified Warthin-Starry staining for melanin detection (Joly-Tonetti et al., 2016). To detect senescent cells (Dimri et al., 1995), Senescence Associated β-galactosidase staining kit (Cell Signaling, Danvers, MA) was used. The number of mast cells and senescent cells, as well as semi-automated skin pigmentation analysis were performed per 200X microscopic field using ImageJ software (NIH, Bethesda, MD).

For immunofluorescence, 10 um cryosections were fixed and incubated with primary antibodies (**Table S8**), followed by application of the secondary antibodies, as described previously (Botchkareva et al., 1999, Muller-Rover et al., 1998, Sharov et al., 2003).

Quantification of immunofluorescence intensity or corrected total cell fluorescence (CTCF) was determined using ImageJ software, as described previously (Rapisarda et al., 2017). Statistical analysis was performed using unpaired Student's *t*-test; differences were deemed significant if $p<0.05$.

RNA-seq, qRT-PCR and bioinformatics analyses

Total RNA was extracted from full-thickness dorsal skin samples obtained from young and old animals (4 year-old skin, n=2; 19 year-old skin, n=2) and purified using Direct-zol RNA purification kit (Zymo Research; Irvine, CA) following by DNAse treatment. Integrity of RNA was assessed on 2100 Bioanalyzer Instrument (Agilent Technologies, Inc.), only samples with RIN factor above 7.5 were used for NGS library preparation. For RNA sequencing, approximately 10 ug of total RNA was used to remove ribosomal RNA according to the manuscript of the Epicentre Ribo-Zero Gold Kit (Illumina, San Diego, USA). The pair-end 2×150bp sequencing was performed on an Illumina Hiseq 4000 platform in the LC Sciences (Houston, TX).

qRT-PCR was performed with iQ SYBR Green Supermix (Bio-Rad Laboratories), as described previously (Mardaryev et al., 2014, Mardaryev et al., 2016). The primer sequences (**Table S9**) were obtained from previously published datasets (Tian et al., 2015). Differences between samples were calculated based on the Ct (ΔΔCt) method and normalized to β-actin. Statistical analysis was performed using an unpaired Student's t test.

The detailed description of the bioinformatics and protein-protein interaction network analyses is provided in Supplementary Material.

Data Availability Statement

Datasets related to this article are deposited to GEO (accession number GSE200736) and are publicly accessible.

ORCID IDs

Iqra Fatima https://orcid.org/0000-0003-0610-5797
Guodong Chen https://orcid.org/0000-0001-9399-9252
Natalia V Botchkareva https://orcid.org/0000-0002-5202-6822
Andrey Sharov https://orcid.org/0000-0002-7240-304X
Holly N. Wilkinson https://orcid.org/0000-0002-8453-7264
Matthew J. Hardman https://orcid.org/0000-0002-6423-5074
Andreas Grutzkau https://orcid.org/0000-0001-6490-2992
Joao Pedro de Magalhaes https://orcid.org/0000-0002-6363-2465
Andrei Seluanov https://orcid.org/0000-0003-3400-538X
Ewan St. J. Smith https://orcid.org/0000-0002-2699-1979
Vera Gorbunova https://orcid.org/0000-0001-8979-0333
Chris G. Faulkes https://orcid.org/0000-0002-5228-9075
Andrei N Mardaryev https://orcid.org/0000-0002-7826-5506
Vladimir A. Botchkarev https://orcid.org/0000-0002-5212-5353

Conflict of Interest The authors state no conflicts of interest.

Acknowledgments

Authors thank L. Faulkes for help in preparation of the NMR images for this manuscript. This study was supported in part by the grants from NIAMS to VAB, AS and VG (R61AR078093), NIA to VG and AS, Dunhill Medical Trust (RPGF2002\188) to EStJS. HAGR is supported by a Biotechnology and Biological Sciences Research Council UK (BB/R014949/1) grant to JPM. AG was supported by the Leibniz Science Campus Chronic Inflammation (A.G., www.chronische-entzuendung.org).

Author Contributions

Conceptualization, Data curation – VB, CF, AM
Formal Analysis – IF, GC, NB, AS, DT, JPM, HW
Funding acquisition – VB, AS, VG, EStJS, JPM
Investigation - IF, GC, NB, AS, DT, JPM
Methodology - VB, CF, AM, VG, AS, EStJS, AG
Project administration – VB, AM
Resources – VB, AM, CF, EStJS, AG
Software – AM, JPM
Supervision – VB, AM, MH, JPM
Validation - IF, GC, NB, AS
Writing – original draft – VB, AM
Writing – review & editing CF, EStJS, VG, JPM, MH

References

Ahmed MI, Alam M, Emelianov VU, Poterlowicz K, Patel A, Sharov AA, et al. MicroRNA-214 controls skin and hair follicle development by modulating the activity of the Wnt pathway. J Cell Biol 2014;207(4):549-67.

Aramillo Irizar P, Schauble S, Esser D, Groth M, Frahm C, Priebe S, et al. Transcriptomic alterations during ageing reflect the shift from cancer to degenerative diseases in the elderly. Nat Commun 2018;9(1):327.

Assabban A, Dubois-Vedrenne I, Van Maele L, Salcedo R, Snyder BL, Zhou L, et al. Tristetraprolin expression by keratinocytes protects against skin carcinogenesis. JCI Insight 2021;6(5).

Balasubramanian S, Ahmad N, Mukhtar H. Upregulation of E2F transcription factors in chemically induced mouse skin tumors. Int J Oncol 1999;15(2):387-90.

Barron CC, Bilan PJ, Tsakiridis T, Tsiani E. Facilitative glucose transporters: Implications for cancer detection, prognosis and treatment. Metabolism 2016;65(2):124-39.

Barth E, Srivastava A, Stojiljkovic M, Frahm C, Axer H, Witte OW, et al. Conserved aging-related signatures of senescence and inflammation in different tissues and species. Aging (Albany NY) 2019;11(19):8556-72.

Bonnans C, Chou J, Werb Z. Remodelling the extracellular matrix in development and disease. Nat Rev Mol Cell Biol 2014;15(12):786-801.

Botchkarev VA. The Molecular Revolution in Cutaneous Biology: Chromosomal Territories, Higher-Order Chromatin Remodeling, and the Control of Gene Expression in Keratinocytes. J Invest Dermatol 2017;137(5):e93-e9.

Botchkarev VA, Botchkarev NV, Albers KM, van der Veen C, Lewin GR, Paus R. Neurotrophin-3 involvement in the regulation of hair follicle morphogenesis. J Invest Dermatol 1998;111(2):279-85.

Botchkarev VA, Botchkareva NV, Roth W, Nakamura M, Chen LH, Herzog W, et al. Noggin is a mesenchymally derived stimulator of hair-follicle induction. Nat Cell Biol 1999;1(3):158-64.

Botchkarev VA, Flores ER. p53/p63/p73 in the epidermis in health and disease. Cold Spring Harb Perspect Med 2014;4(8).

Botchkarev VA, Gdula MR, Mardaryev AN, Sharov AA, Fessing MY. Epigenetic regulation of gene expression in keratinocytes. J Invest Dermatol 2012;132(11):2505-21.

Botchkareva NV, Botchkarev VA, Chen LH, Lindner G, Paus R. A role for p75 neurotrophin receptor in the control of hair follicle morphogenesis. Dev Biol 1999;216(1):135-53.

Braude S, Holtze S, Begall S, Brenmoehl J, Burda H, Dammann P, et al. Surprisingly long survival of premature conclusions about naked mole-rat biology. Biol Rev Camb Philos Soc 2021;96(2):376-93.

Brohus M, Gorbunova V, Faulkes CG, Overgaard MT, Conover CA. The Insulin-Like Growth Factor System in the Long-Lived Naked Mole-Rat. PLoS One 2015;10(12):e0145587.

Buccitelli C, Selbach M. mRNAs, proteins and the emerging principles of gene expression control. Nat Rev Genet 2020;21(10):630-44.

Buffenstein R. The naked mole-rat: a new long-living model for human aging research. J Gerontol A Biol Sci Med Sci 2005;60(11):1369-77.

Buffenstein R, Amoroso V, Andziak B, Avdieiev S, Azpurua J, Barker AJ, et al. The naked truth: a comprehensive clarification and classification of current 'myths' in naked mole-rat biology. Biol Rev Camb Philos Soc 2021.

Chuong CM, Nickoloff BJ, Elias PM, Goldsmith LA, Macher E, Maderson PA, et al. What is the 'true' function of skin? Exp Dermatol 2002;11(2):159-87.

Cole MA, Quan T, Voorhees JJ, Fisher GJ. Extracellular matrix regulation of fibroblast function: redefining our perspective on skin aging. J Cell Commun Signal 2018;12(1):35-43.

Crosara KTB, Moffa EB, Xiao Y, Siqueira WL. Merging in-silico and in vitro salivary protein complex partners using the STRING database: A tutorial. J Proteomics 2018;171:87-94.

Daly TJ, Buffenstein R. Skin morphology and its role in thermoregulation in mole-rats, Heterocephalus glaber and Cryptomys hottentotus. J Anat 1998;193 (Pt 4):495-502.

Del Marmol D, Holtze S, Kichler N, Sahm A, Bihin B, Bourguignon V, et al. Abundance and size of hyaluronan in naked mole-rat tissues and plasma. Sci Rep 2021;11(1):7951.

Delaney MA, Nagy L, Kinsel MJ, Treuting PM. Spontaneous histologic lesions of the adult naked mole rat (Heterocephalus glaber): a retrospective survey of lesions in a zoo population. Vet Pathol 2013;50(4):607-21.

Dimri GP, Lee X, Basile G, Acosta M, Scott G, Roskelley C, et al. A biomarker that identifies senescent human cells in culture and in aging skin in vivo. Proc Natl Acad Sci U S A 1995;92(20):9363-7.

Evdokimov A, Kutuzov M, Petruseva I, Lukjanchikova N, Kashina E, Kolova E, et al. Naked mole rat cells display more efficient excision repair than mouse cells. Aging (Albany NY) 2018;10(6):1454-73.

Fessing MY, Mardaryev AN, Gdula MR, Sharov AA, Sharova TY, Rapisarda V, et al. p63 regulates Satb1 to control tissue-specific chromatin remodeling during development of the epidermis. J Cell Biol 2011;194(6):825-39.

Ge Y, Miao Y, Gur-Cohen S, Gomez N, Yang H, Nikolova M, et al. The aging skin microenvironment dictates stem cell behavior. Proc Natl Acad Sci U S A 2020;117(10):5339-50.

Gladyshev VN, Zhang G, Wang J. The naked mole rat genome: understanding aging through genome analysis. Aging (Albany NY) 2011;3(12):1124.

Gorbunova V, Seluanov A, Zhang Z, Gladyshev VN, Vijg J. Comparative genetics of longevity and cancer: insights from long-lived rodents. Nat Rev Genet 2014;15(8):531-40.

Gunin AG, Petrov VV, Golubtzova NN, Vasilieva OV, Kornilova NK. Age-related changes in angiogenesis in human dermis. Exp Gerontol 2014;55:143-51.

He B, Zhu R, Yang H, Lu Q, Wang W, Song L, et al. Assessing the Impact of Data Preprocessing on Analyzing Next Generation Sequencing Data. Front Bioeng Biotechnol 2020;8:817.

Horvath S, Haghani A, Macoretta N, Ablaeva J, Zoller JA, Li CZ, et al. DNA methylation clocks tick in naked mole rats but queens age more slowly than nonbreeders. Nature Aging 2022;2:46-59.

Jenkins BA, Fontecilla NM, Lu CP, Fuchs E, Lumpkin EA. The cellular basis of mechanosensory Merkel-cell innervation during development. Elife 2019;8.

Joly-Tonetti N, Wibawa JI, Bell M, Tobin D. Melanin fate in the human epidermis: a reassessment of how best to detect and analyse histologically. Exp Dermatol 2016;25(7):501-4.

Keyes BE, Segal JP, Heller E, Lien WH, Chang CY, Guo X, et al. Nfatc1 orchestrates aging in hair follicle stem cells. Proc Natl Acad Sci U S A 2013;110(51):E4950-9.

Kim EB, Fang X, Fushan AA, Huang Z, Lobanov AV, Han L, et al. Genome sequencing reveals insights into physiology and longevity of the naked mole rat. Nature 2011;479(7372):223-7.

Koster MI, Dai D, Roop DR. Conflicting roles for p63 in skin development and carcinogenesis. Cell Cycle 2007;6(3):269-73.

Kouwenhoven EN, Oti M, Niehues H, van Heeringen SJ, Schalkwijk J, Stunnenberg HG, et al. Transcription factor p63 bookmarks and regulates dynamic enhancers during epidermal differentiation. EMBO Rep 2015;16(7):863-78.

Kulaberoglu Y, Bhushan B, Hadi F, Chakrabarti S, Khaled WT, Rankin KS, et al. The material properties of naked mole-rat hyaluronan. Sci Rep 2019;9(1):6632.

Langton AK, Graham HK, Watson RE. Diverse methodologies for assessing photoaged skin. Br J Dermatol 2016;174(3):487-8.

Langton AK, Sherratt MJ, Griffiths CE, Watson RE. A new wrinkle on old skin: the role of elastic fibres in skin ageing. Int J Cosmet Sci 2010;32(5):330-9.

Larsen SB, Cowley CJ, Fuchs E. Epithelial cells: liaisons of immunity. Curr Opin Immunol 2020;62:45-53.

Lewis DA, Travers JB, Somani AK, Spandau DF. The IGF-1/IGF-1R signaling axis in the skin: a new role for the dermis in aging-associated skin cancer. Oncogene 2010;29(10):1475-85.

Liu N, Matsumura H, Kato T, Ichinose S, Takada A, Namiki T, et al. Stem cell competition orchestrates skin homeostasis and ageing. Nature 2019;568(7752):344-50.

Lowe R, Danson AF, Rakyan VK, Yildizoglu S, Saldmann F, Viltard M, et al. DNA methylation clocks as a predictor for ageing and age estimation in naked mole-rats, Heterocephalus glaber. Aging (Albany NY) 2020;12(5):4394-406.

MacRae SL, Zhang Q, Lemetre C, Seim I, Calder RB, Hoeijmakers J, et al. Comparative analysis of genome maintenance genes in naked mole rat, mouse, and human. Aging Cell 2015;14(2):288-91.

Mardaryev AN, Gdula MR, Yarker JL, Emelianov VU, Poterlowicz K, Sharov AA, et al. p63 and Brg1 control developmentally regulated higher-order chromatin remodelling at the epidermal differentiation complex locus in epidermal progenitor cells. Development 2014;141(1):101-11.

Mardaryev AN, Liu B, Rapisarda V, Poterlowicz K, Malashchuk I, Rudolf J, et al. Cbx4 maintains the epithelial lineage identity and cell proliferation in the developing stratified epithelium. J Cell Biol 2016;212(1):77-89.

Martins R, Lithgow GJ, Link W. Long live FOXO: unraveling the role of FOXO proteins in aging and longevity. Aging Cell 2016;15(2):196-207.

Menon GK, Catania KC, Crumrine D, Bradley C, Mauldin EA. Unique features of the skin barrier in naked mole rats reflect adaptations to their fossorial habitat. J Morphol 2019;280(12):1871-80.

Menon GK, Kligman AM. Barrier functions of human skin: a holistic view. Skin Pharmacol Physiol 2009;22(4):178-89.

Muller-Rover S, Peters EJ, Botchkarev VA, Panteleyev A, Paus R. Distinct patterns of NCAM expression are associated with defined stages of murine hair follicle morphogenesis and regression. J Histochem Cytochem 1998;46(12):1401-10.

Parry A, Rulands S, Reik W. Active turnover of DNA methylation during cell fate decisions. Nat Rev Genet 2021;22(1):59-66.

Pilkington SM, Bulfone-Paus S, Griffiths CEM, Watson REB. Inflammaging and the Skin. J Invest Dermatol 2021;141(4S):1087-95.
Qu J, Yi G, Zhou H. p63 cooperates with CTCF to modulate chromatin architecture in skin keratinocytes. Epigenetics Chromatin 2019;12(1):31.
Raddatz G, Hagemann S, Aran D, Sohle J, Kulkarni PP, Kaderali L, et al. Aging is associated with highly defined epigenetic changes in the human epidermis. Epigenetics Chromatin 2013;6(1):36.
Rapisarda V, Malashchuk I, Asamaowei IE, Poterlowicz K, Fessing MY, Sharov AA, et al. p63 Transcription Factor Regulates Nuclear Shape and Expression of Nuclear Envelope-Associated Genes in Epidermal Keratinocytes. J Invest Dermatol 2017;137(10):2157-67.
Ressler S, Bartkova J, Niederegger H, Bartek J, Scharffetter-Kochanek K, Jansen-Durr P, et al. p16INK4A is a robust in vivo biomarker of cellular aging in human skin. Aging Cell 2006;5(5):379-89.
Rittie L, Fisher GJ. UV-light-induced signal cascades and skin aging. Ageing Res Rev 2002;1(4):705-20.
Rittie L, Fisher GJ. Natural and sun-induced aging of human skin. Cold Spring Harb Perspect Med 2015;5(1):a015370.
Rodriguez KA, Valentine JM, Kramer DA, Gelfond JA, Kristan DM, Nevo E, et al. Determinants of rodent longevity in the chaperone-protein degradation network. Cell Stress Chaperones 2016;21(3):453-66.
Rognoni E, Watt FM. Skin Cell Heterogeneity in Development, Wound Healing, and Cancer. Trends Cell Biol 2018;28(9):709-22.
Rood BR, Leprince D. Deciphering HIC1 control pathways to reveal new avenues in cancer therapeutics. Expert Opin Ther Targets 2013;17(7):811-27.
Rosset C, Netto CBO, Ashton-Prolla P. TSC1 and TSC2 gene mutations and their implications for treatment in Tuberous Sclerosis Complex: a review. Genet Mol Biol 2017;40(1):69-79.
Savina A, Jaffredo T, Saldmann F, Faulkes CG, Moguelet P, Leroy C, et al. Epidermal stem cell compartment remains unaffected through aging in naked mole-rats. BioRxiv 2020:doi: https://doi.org/10.1101/2020.11.13.381061.
Seluanov A, Gladyshev VN, Vijg J, Gorbunova V. Mechanisms of cancer resistance in long-lived mammals. Nat Rev Cancer 2018;18(7):433-41.
Sharov AA, Li GZ, Palkina TN, Sharova TY, Gilchrest BA, Botchkarev VA. Fas and c-kit are involved in the control of hair follicle melanocyte apoptosis and migration in chemotherapy-induced hair loss. J Invest Dermatol 2003;120(1):27-35.
Shebzukhov Y, Holtze S, Hirseland H, Schafer H, Radbruch A, Hildebrandt T, et al. Identification of cross-reactive antibodies for the detection of lymphocytes, myeloid cells and haematopoietic precursors in the naked mole rat. Eur J Immunol 2019;49(11):2103-10.
Slominski AT, Zmijewski MA, Skobowiat C, Zbytek B, Slominski RM, Steketee JD. Sensing the environment: regulation of local and global homeostasis by the skin's neuroendocrine system. Adv Anat Embryol Cell Biol 2012;212:v, vii, 1-115.
Smith ESJ, Park TJ, Lewin GR. Independent evolution of pain insensitivity in African mole-rats: origins and mechanisms. J Comp Physiol A Neuroethol Sens Neural Behav Physiol 2020;206(3):313-25.
Sondka Z, Bamford S, Cole CG, Ward SA, Dunham I, Forbes SA. The COSMIC Cancer Gene Census: describing genetic dysfunction across all human cancers. Nat Rev Cancer 2018;18(11):696-705.

Stacpoole PW. The pyruvate dehydrogenase complex as a therapeutic target for age-related diseases. Aging Cell 2012;11(3):371-7.
Su X, Paris M, Gi YJ, Tsai KY, Cho MS, Lin YL, et al. TAp63 prevents premature aging by promoting adult stem cell maintenance. Cell Stem Cell 2009;5(1):64-75.
Tacutu R, Thornton D, Johnson E, Budovsky A, Barardo D, Craig T, et al. Human Ageing Genomic Resources: new and updated databases. Nucleic Acids Res 2018;46(D1):D1083-D90.
Takasugi M, Firsanov D, Tombline G, Ning H, Ablaeva J, Seluanov A, et al. Naked mole-rat very-high-molecular-mass hyaluronan exhibits superior cytoprotective properties. Nat Commun 2020;11(1):2376.
Thigpen LW. Histology of the Skin of a Normally Hairless Rodent. J Mammalogy 1940;21(4):449-56.
Tian X, Azpurua J, Ke Z, Augereau A, Zhang ZD, Vijg J, et al. INK4 locus of the tumor-resistant rodent, the naked mole rat, expresses a functional p15/p16 hybrid isoform. Proc Natl Acad Sci U S A 2015;112(4):1053-8.
Toutfaire M, Bauwens E, Debacq-Chainiaux F. The impact of cellular senescence in skin ageing: A notion of mosaic and therapeutic strategies. Biochem Pharmacol 2017;142:1-12.
Tucker R. The digging behavior and skin differentiations in Heterocephalus glaber. J Morphol 1981;168(1):51-71.
Victorelli S, Lagnado A, Halim J, Moore W, Talbot D, Barrett K, et al. Senescent human melanocytes drive skin ageing via paracrine telomere dysfunction. EMBO J 2019;38(23):e101982.
Waaijer ME, Gunn DA, Adams PD, Pawlikowski JS, Griffiths CE, van Heemst D, et al. P16INK4a Positive Cells in Human Skin Are Indicative of Local Elastic Fiber Morphology, Facial Wrinkling, and Perceived Age. J Gerontol A Biol Sci Med Sci 2016;71(8):1022-8.
Waaijer ME, Parish WE, Strongitharm BH, van Heemst D, Slagboom PE, de Craen AJ, et al. The number of p16INK4a positive cells in human skin reflects biological age. Aging Cell 2012;11(4):722-5.
Waaijer MEC, Gunn DA, van Heemst D, Slagboom PE, Sedivy JM, Dirks RW, et al. Do senescence markers correlate in vitro and in situ within individual human donors? Aging (Albany NY) 2018;10(2):278-89.
Watt B, van Niel G, Raposo G, Marks MS. PMEL: a pigment cell-specific model for functional amyloid formation. Pigment Cell Melanoma Res 2013;26(3):300-15.
Winkler GS. The mammalian anti-proliferative BTG/Tob protein family. J Cell Physiol 2010;222(1):66-72.
Yaar M, Eller MS, Gilchrest BA. Fifty years of skin aging. J Investig Dermatol Symp Proc 2002;7(1):51-8.
Zhao Y, Tyshkovskiy A, Munoz-Espin D, Tian X, Serrano M, de Magalhaes JP, et al. Naked mole rats can undergo developmental, oncogene-induced and DNA damage-induced cellular senescence. Proc Natl Acad Sci U S A 2018;115(8):1801-6.

Figure Legends

Figure 1. Visual appearance of the skin and age-related changes in the epidermis of NMRs.

a – Images of the skin in 3- and 23-year-old animals, note the more translucent and less pigmented dorsal skin in aged NMR. **b** – Hematoxylin/eosin staining of the young and old skin: presence of the dermal pigment (arrow) in young skin and significantly reduced epidermal thickness in old animals. **c –** Significant decrease in Ki67+ cells in aged versus young NMRs. **d-f** - Significantly decreased immunofluorescence intensity of K14 in the basal layer (**d**), K10 in the spinous layer (**e**), and Loricrin in the granular layer (**f**) in the epidermis of old NMRs. **g** - Significant decrease in the immunofluorescence intensity of p63 in epidermal keratinocytes of old versus young NMRs. **h** – Significant decline in the expression of COL17A1 in basal epidermal keratinocytes and dermal-epidermal basement membrane of old animals. **i** – Significant decrease in the number of KRT20+ Merkel cells in the epidermis of old NMRs (arrows). (mean ± SD, *$p<0.05$, Student's t-test. Scale bars, 100 µm (b), 25 µm (c – i). Y – young animal, O – old animal.

Figure 2. Age-associated changes in the NMR dermis.

(a) Significantly reduced number of epidermal buds elongating into the dermis (arrows) in the aged NMR skin. **(b)** Similar distribution of Fibrillin-2+ fibers in young and old NMRs. **(c)** COL1A1 is broadly expressed in the papillary and reticular dermis of young NMRs, while COL1A1 expression is significantly decreased in the reticular dermis in aged skin. **(d)** Significant increase in the MMP9 immunofluorescence intensity in the dermis of old NMRs compared to young animals. **(e)** No differences in the hyaluronan-binding protein (HA-BP) binding pattern or degree of binding between the dermis of young and old NMRs. **(f)** Similar expression of the HA receptor CD44 in the skin of young and old NMRs. **(g)** Warthin-Starry stain shows a dramatic decrease in the melanin containing areas in the dermis of old compared to young NMRs, which is

accompanied by a significant decrease in the number of gp100+ pigment-producing dermal melanocytes in the dermis of aged animals **(h**, arrows). Mean ± SD, *p<0.05, Student's t-test. Scale bars, 25 μm. Y – young animal, O – old animal.

Figure 3. Aging-associated changes in the number of immune and senescent cells in the NMR skin.

(a) Significant decrease in the number of CD3ε+ T-cells in the epidermis of old NMRs. **(b)** Significant decrease in the number of MHC II+ cells detected by an anti-27E7 antibody in the epidermis and dermis of old NMRs. **(c)** No changes in the number of CD8+ cells in the dermis of aged versus young NMRs (arrows). **(d)** The number of dermal CD11b+ macrophages is similar in the young and old NMRs. **(e)** Significant increase in the number of senescent SA-β-gal+ cells (arrow) in the epidermis of old NMRs. A tendentious, but not significant, increase in the number of SA-β-gal+ cells (arrows) in the aged dermis (p=0.082). Mean ± SD, *p<0.05, Student's t-test. Scale bars, 25 μm. Y – young animal, O – old animal.

Figure 4. RNAseq analyses of the age-associated changes in the cutaneous NMR transcriptome.

(a) Functional annotation of the differentially expressed genes based on QIAGEN Ingenuity Pathway Analysis database and manually curated functional gene sub-categories. **(b)** A list of five top differentially expressed genes in each functional group (fold-change expression values are indicated by asterisks). **(c)** GO enrichment analysis showed significant over-representation of the extracellular matrix-associated genes, components of the insulin growth factor (IGF) signaling pathway, regulators of the glucose metabolism and cell proliferation.

Figure 5. Comparison of age-associated changes in the transcriptome of NMR, human, and mouse skin

(a) The number of differentially expressed genes common between the NMR skin aging transcriptome and the Human Ageing Genome Resource (HAGR) genes (here denoted as aging signature genes) relative to the total number of differentially expressed genes; **(b)** The number of differentially expressed genes common between the NMR skin aging transcriptome and the Cancer Gene Census (CGC)/Tumor Suppressor Genes (TSG) datasets (here denoted as cancer signature genes) relative to the total number of differentially expressed genes; **(c)** A Venn diagram shows the differentially expressed genes in the NMR skin aging transcriptome that are shared with the human HAGR and CGC/TSG databases. Comparative analyses of gene expression (old versus young) in the skin of three species: NMR (total skin), human (total skin, epidermis) and mouse (total skin, FACS-sorted basal epidermal keratinocytes). The differences in gene expression are shown as the FPKM fold-change.

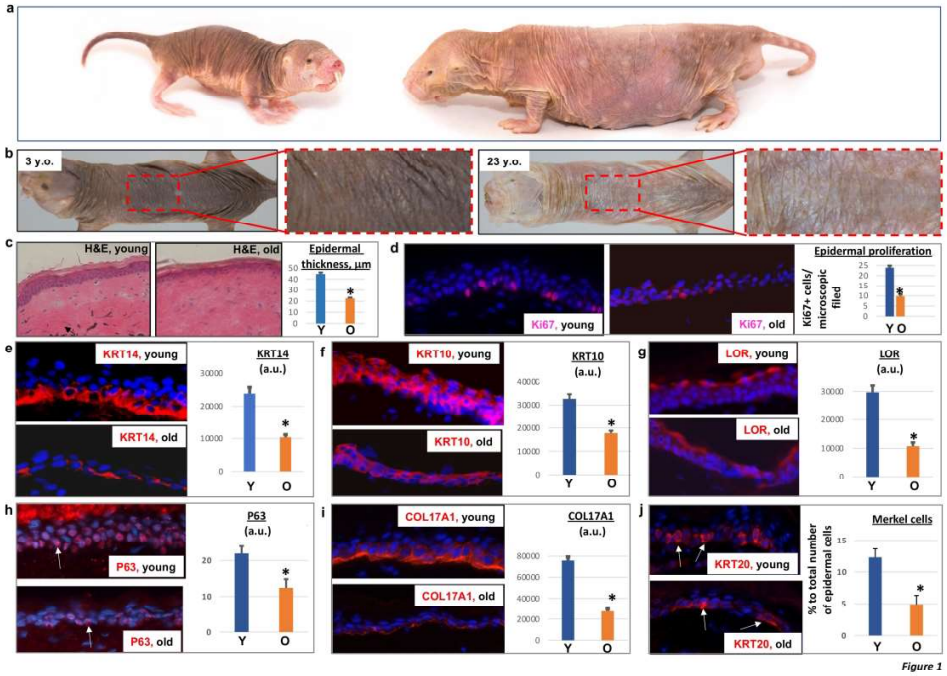
a
b
3 y.o.
23 y.o.
c
H&E, young
H&E, old
Epidermal thickness, µm
d
Ki67, young
Ki67, old
Epidermal proliferation
Ki67+ cells/ microscopic filed
e
KRT14, young
KRT14, old
KRT14 (a.u.)
f
KRT10, young
KRT10, old
KRT10 (a.u.)
g
LOR, young
LOR, old
LOR (a.u.)
h
P63, young
P63, old
P63 (a.u.)
i
COL17A1, young
COL17A1, old
COL17A1 (a.u.)
j
KRT20, young
KRT20, old
Merkel cells
% to total number of epidermal cells
Y
O

Figure 1

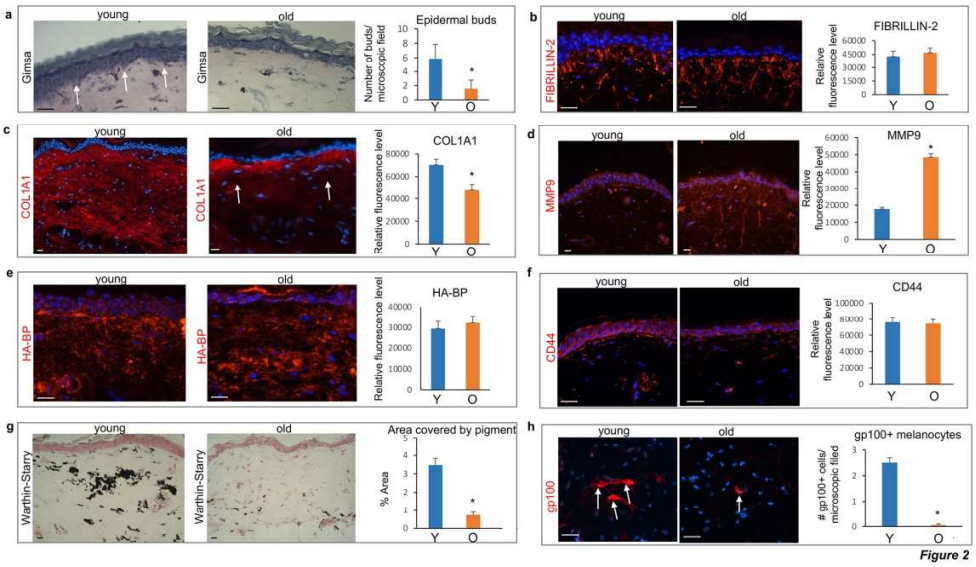
a
young
old
Gimsa
Epidermal buds
Number of buds/ microscopic field
b
FIBRILLIN-2
Relative fluorescence level
c
COL1A1
d
MMP9
e
HA-BP
f
CD44
g
Warthin-Starry
Area covered by pigment
% Area
h
gp100
gp100+ melanocytes
gp100+ cells/ microscopic filed
Y
O
Figure 2

Figure 2

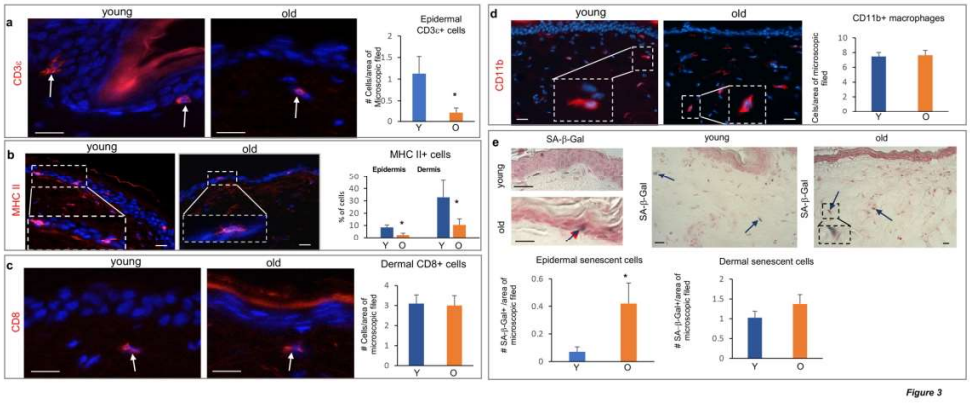
a
young
old
CD3ε
Epidermal CD3ε+ cells
Cells/area of Microscopic field
Y
O
b
young
old
MHC II
MHC II+ cells
Epidermis
Dermis
% of cells
c
young
old
CD8
Dermal CD8+ cells
Cells/area of microscopic field
d
young
old
CD11b
CD11b+ macrophages
Cells/area of microscopic field
e
SA-β-Gal
young
old
Epidermal senescent cells
SA-β-Gal+ /area of microscopic field
Dermal senescent cells
SA-β-Gal+/area of microscopic field
Figure 3

Figure 3

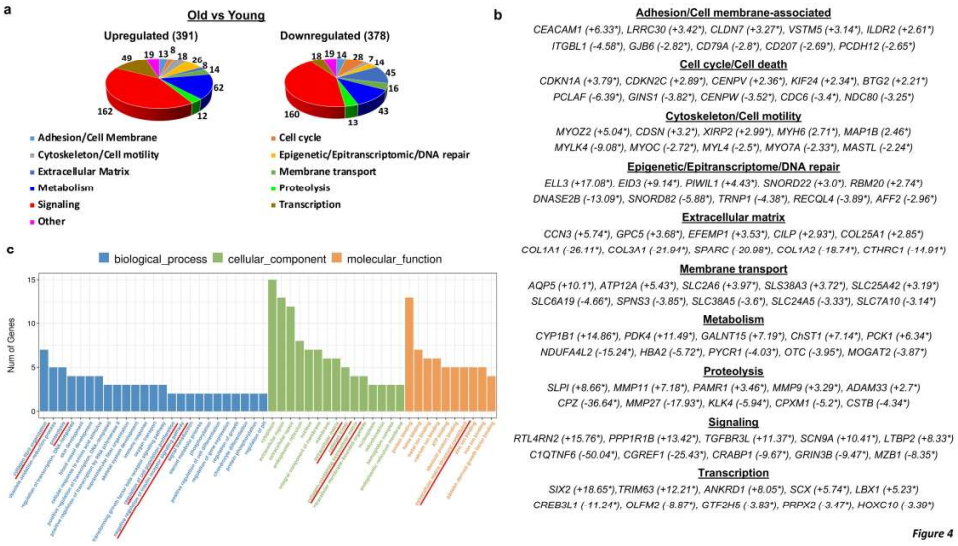
a
Old vs Young
Upregulated (391)
Downregulated (378)
Adhesion/Cell Membrane
Cytoskeleton/Cell motility
Extracellular Matrix
Metabolism
Signaling
Other
Cell cycle
Epigenetic/Epitranscriptomic/DNA repair
Membrane transport
Proteolysis
Transcription
b
Adhesion/Cell membrane-associated
CEACAM1 (+6.33*), LRRC30 (+3.42*), CLDN7 (+3.27*), VSTM5 (+3.14*), ILDR2 (+2.61*)
ITGBL1 (-4.58*), GJB6 (-2.82*), CD79A (-2.8*), CD207 (-2.69*), PCDH12 (-2.65*)
Cell cycle/Cell death
CDKN1A (+3.79*), CDKN2C (+2.89*), CENPV (+2.36*), KIF24 (+2.34*), BTG2 (+2.21*)
PCLAF (-6.39*), GINS1 (-3.82*), CENPW (-3.52*), CDC6 (-3.4*), NDC80 (-3.25*)
Cytoskeleton/Cell motility
MYOZ2 (+5.04*), CDSN (+3.2*), XIRP2 (+2.99*), MYH6 (2.71*), MAP1B (2.46*)
MYLK4 (-9.08*), MYOC (-2.72*), MYL4 (-2.5*), MYO7A (-2.33*), MASTL (-2.24*)
Epigenetic/Epitranscriptome/DNA repair
ELL3 (+17.08*), EID3 (+9.14*), PIWIL1 (+4.43*), SNORD22 (+3.0*), RBM20 (+2.74*)
DNASE2B (-13.09*), SNORD82 (-5.88*), TRNP1 (-4.38*), RECQL4 (-3.89*), AFF2 (-2.96*)
Extracellular matrix
CCN3 (+5.74*), GPC5 (+3.68*), EFEMP1 (+3.53*), CILP (+2.93*), COL25A1 (+2.85*)
COL1A1 (-26.11*), COL3A1 (-21.94*), SPARC (-20.98*), COL1A2 (-18.74*), CTHRC1 (-11.91*)
Membrane transport
AQP5 (+10.1*), ATP12A (+5.43*), SLC2A6 (+3.97*), SLS38A3 (+3.72*), SLC25A42 (+3.19*)
SLC6A19 (-4.66*), SPNS3 (-3.85*), SLC38A5 (-3.6*), SLC24A5 (-3.33*), SLC7A10 (-3.14*)
Metabolism
CYP1B1 (+14.86*), PDK4 (+11.49*), GALNT15 (+7.19*), ChST1 (+7.14*), PCK1 (+6.34*)
NDUFA4L2 (-15.24*), HBA2 (-5.72*), PYCR1 (-4.03*), OTC (-3.95*), MOGAT2 (-3.87*)
Proteolysis
SLPI (+8.66*), MMP11 (+7.18*), PAMR1 (+3.46*), MMP9 (+3.29*), ADAM33 (+2.7*)
CPZ (-36.64*), MMP27 (-17.93*), KLK4 (-5.94*), CPXM1 (-5.2*), CSTB (-4.34*)
Signaling
RTL4RN2 (+15.76*), PPP1R1B (+13.42*), TGFBR3L (+11.37*), SCN9A (+10.41*), LTBP2 (+8.33*)
C1QTNF6 (-50.04*), CGREF1 (-25.43*), CRABP1 (-9.67*), GRIN3B (-9.47*), MZB1 (-8.35*)
Transcription
SIX2 (+18.65*),TRIM63 (+12.21*), ANKRD1 (+8.05*), SCX (+5.74*), LBX1 (+5.23*)
CREB3L1 (-11.24*), OLFM2 (-8.87*), GTF2H5 (-3.83*), PRPX2 (-3.47*), HOXC10 (-3.39*)
c
biological_process
cellular_component
molecular_function
Num of Genes
Figure 4

Figure 4

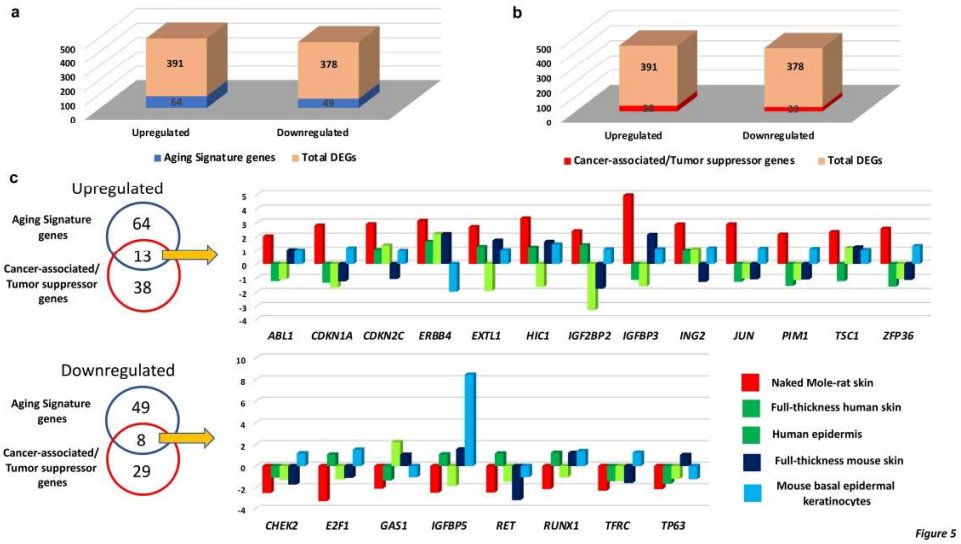
a
500
400
300
200
100
0
391
378
64
49
Upregulated
Downregulated
Aging Signature genes
Total DEGs
b
391
378
38
29
Upregulated
Downregulated
Cancer-associated/Tumor suppressor genes
Total DEGs
c
Upregulated
Aging Signature genes
Cancer-associated/ Tumor suppressor genes
64
13
38
ABL1
CDKN1A
CDKN2C
ERBB4
EXTL1
HIC1
IGF2BP2
IGFBP3
ING2
JUN
PIM1
TSC1
ZFP36
Downregulated
Aging Signature genes
Cancer-associated/ Tumor suppressor genes
49
8
29
CHEK2
E2F1
GAS1
IGFBP5
RET
RUNX1
TFRC
TP63
Naked Mole-rat skin
Full-thickness human skin
Human epidermis
Full-thickness mouse skin
Mouse basal epidermal keratinocytes
Figure 5

Figure 5

Supplementary Material

Materials & Methods

Quantification of immunofluorescence intensity. Red or green fluorescent signal was collected from experimental tissues in RGB format using the same exposure conditions. Regions of interest of distinct size within the epidermis or dermis were selected, and CTCF value was quantified using integrated density of the immunofluorescence against the area of selected region and mean gray value of the background. At least 10 40x-images per group with exactly the same image acquisition parameters have been taken. Statistical analysis was performed using unpaired Student's t-test; differences were deemed significant if $p<0.05$.

We used a complex approach to avoid significant errors in quantification of fluorescence intensity: i) To avoid the errors derived from the UV source, the fluorescence bulbs were regularly replaced before reaching their max lifespan by a qualified technician.

ii) To minimize the issue related to the fading of fluorescent dyes, we used Alexa-coupled secondary antibodies. Alexa dyes are proven to be more photostable than their commonly used fluorophores (N Panchuk-Voloshina et al. *Alexa dyes, a series of new fluorescent dyes that yield exceptionally bright, photostable conjugates*. J Histochem Cytochem. 1999, 47:1179-88). With maintaining the same exposure conditions that were set to avoid over- and under-saturation, an area of imaging was exposed only once for a very short time required to capture the image. Acquiring images for each immunofluorescence protocol (each antibody), including both age groups, was performed by the same person during one imaging session. Monochrome greyscale images were acquired with QIMAGING RETIGA EXI AQUA MONO camera, which supports low light fluorescent imaging, with enhanced sensitivity, high resolution, and broad spectral response (https://www.mediacy.com/support/imagepro/hardware). For illustration purpose, each greyscale

image channel was pseudo-colored and merged to produce colored images in RGB format with the Image Pro Insight 9.0 software.

iii) For image analysis, background correction for total fluorescence correction was performed. Analysis of pixel intensity values was done on raw flat-field grayscale 16-bit TIFF images that preserves the linear relationship between the photons and image intensity values.

RNA extraction and RNA-seq analyses. For RNA sequencing, approximately 10 ug of total RNA was used to remove ribosomal RNA according to the manuscript of the Epicentre Ribo-Zero Gold Kit (Illumina, San Diego, USA). Following purification, the ribo-minus RNA fractions is fragmented into small pieces using divalent cations under elevated temperature. Then the cleaved RNA fragments were reverse-transcribed to create the final cDNA library in accordance with a strand-specific library preparation by dUTP method. The average insert size for the paired-end libraries was 300±50 bp. The pair-end 2×150bp sequencing was performed on an Illumina Hiseq 4000 platform in the LC Sciences (Houston, TX).

Bioinformatics and protein-protein interaction network analyses. The bioinformatics analysis of the RNAseq data was performed by the LC Sciences (Houston, TX). Firstly, Cutadapt (Martin, 2011) and Perl scripts were used to remove the reads that contained adaptor contamination, low quality bases and undetermined bases. Then, sequence quality was verified using FastQC (http://www.bioinformatics.babraham.ac.uk/projects/fastqc/). Bowtie2 (Langmead and Salzberg, 2012) and Tophat2 (Kim et al., 2013) were used to map reads to the genome of Heterocephalus glaber (https://useast.ensembl.org/Heterocephalus_glaber_female/Info/Index). The differentially expressed mRNAs were selected with log2 (fold change) >1 or log2 (fold change) <-1 and with parametric F-test comparing nested linear models (p value < 0.05) by R package Ballgown. Ballgown was used to generate a list and heatmaps of differentially expressed genes, and in-house generated Perl scripts (LC Science, Houston, TX) were used for Gene Ontology (GO) and

Kyoto Encyclopedia of Genes and Genomes (KEGG) pathway enrichment analyses. In addition, to cluster differentially expressed genes into different functional groups, the QIAGEN Ingenuity Pathway Analysis (QIAGEN IPA) was used (https://digitalinsights.qiagen.com/products-overview/discovery-insights-portfolio/analysis-and-visualization/qiagen-ipa/) as a general platform, and skin-relevant functional gene sub-categories were manually organized accordingly to previously published data (Sharov et al., 2009, Sharov et al., 2006). Also, for each time interval, the significantly differentially expressed genes were input into HAGR (https://genomics.senescence.info/) or CGC (https://cancer.sanger.ac.uk/census) databases. In addition, ClusterProfiler R Package was used to identify KEGG Pathway enrichment and GO functional term enrichment for each of the gene sets.

To predict functional interaction of proteins encoded by differentially expressed genes in young and aged NMRs, the search tool for retrieval of interacting genes (STRING) (https://string-db.org, vision 11.0) database was employed. Active interaction sources, including text mining, experiments, databases, and co-expression as well as species limited to “Heterocephalus glaber” and an interaction score > 0.4 were applied to construct the PPI networks. GO and KEGG pathways were selected with the threshold of adjusted p-value < 0.05.

Supplementary Figure legends

Supplementary Figure S1. Characterization of young and old NMR skin

a) A quantitative analysis of active Caspase 3+ cells: no difference in expression levels between the epidermis of young and old NMRs; **b)** COL3A1 expression in the upper dermis of old NMRs: no difference in total expression levels between young and old animals; **c)** Distribution of dermal elastic fibers and Elastin expression levels are similar between the dermis of young and old animals; **d)** epidermal MMP1 expression with equal immunofluorescence intensity between young and old animals; **e)** Marked increase of MMP11 immunofluorescence in the dermis of old NMRs compared to young animals; **f)** a significant decrease in the number of CD3ε+ T-cells in the dermis of aged NMR skin; **h)** a significant decline in the number of mast cells in aged NMR skin as detected by Gimsa stain; **g)** qRT-PCR: upregulation of $p16^{INK4a}$ in aged vs young full-thickness skin samples, and similar levels of $p15^{INK4b}$ and $pALT^{INK4a/b}$ are seen in old and young skin. Mean ± SD, *p<0.01, Student's t-test. A.u. – arbitrary units, Y – young animal, O – old animal

Supplementary Figure S2. The correlation of the age-associated changes in the NMR skin transcriptome to human or mouse skin aging

Age-associated transcriptome from NMR skin was compared to the transcriptome data from aged human and mouse skin obtained from publicly available datasets (Aramillo Irizar et al. Nature Commun, 2018, 9, 327; Barth et al. Aging, 2019, 11, 8556).

a) Number of genes upregulated during aging in the NMR skin showing similarities or differences in expression in comparison to human or mouse skin aging.

b) Number of genes downregulated during aging in the NMR skin showing similarities or differences in expression in comparison to human or mouse skin aging.

Supplementary Figure S3. Validation of the changes in the NMR skin aging transcriptome by immunofluorescence

a-c) Significant increase of CDKN1A **(a)**, BTG2 (**b)** and TOB1 (**c)** immunofluorescence in the epidermis of aged NMR skin. Mean ± SD, *p<0.01, Student's t-test. A.u. – arbitrary units, Y – young animal, O – old animal.

Supplementary Figure S4. The STRING protein-protein interaction network analysis showing associations among the genes upregulated in the aged NMR skin and longevity-associated genes present in HAGR database

Color nodes represent proteins associated with the corresponding GO term and KEGG pathways, while thickness of the network edges (links) show the strength of data support used for the network reconstruction.

Supplementary Figure S5. The STRING protein-protein interaction network analysis showing associations among the genes downregulated in the aged NMR skin and longevity-associated genes present in HAGR database

Color nodes represent proteins associated with the corresponding GO term and KEGG pathways, while thickness of the network edges (links) show the strength of data support used for the network reconstruction.

Supplementary Figure S6. The STRING protein-protein interaction network analysis showing associations among the genes differentially expressed in the aged NMR skin and cancer-related/tumor suppressor genes present in CGC/TSG databases

Color nodes represent proteins associated with the corresponding GO term and KEGG pathways, while thickness of the network edges (links) show the strength of data support used for the network reconstruction.

Supplementary Tables

Supplementary Table S1. Genes Upregulated in the Skin of Old NMRs vs Young NMRs (RNAseq, FPKM, fold change)

Supplementary Table S2. Genes Downregulated in the Skin of Old NMRs vs Young NMRs (RNAseq, FPKM, fold change)

Supplementary Table S3. Correlation of the RNAseq and quantitative immunofluorescence data for selected markers expressed in young and old NMR skin

Supplementary Table S4. Expression changes of the genes upregulated in old NMR skin in the human and mouse skin during aging (RNAseq, FPKM, fold change)

Supplementary Table S5. Expression changes of the genes downregulated in old NMR skin in the human and mouse skin during aging (RNAseq, FPKM, fold change)

Supplementary Table S6. Genes up- and downregulated in the aged NMR skin and found in the Human Aging Genome Resource (HAGR) database

Supplementary Table S7. Genes up- and downregulated in the aged NMR skin and found in the Cancer Gene Census (CGC) and Tumor Suppressor Genes (TSG) databases

Supplementary Table S8. List of primary antibodies

Supplementary Table 9: List of PCR primers

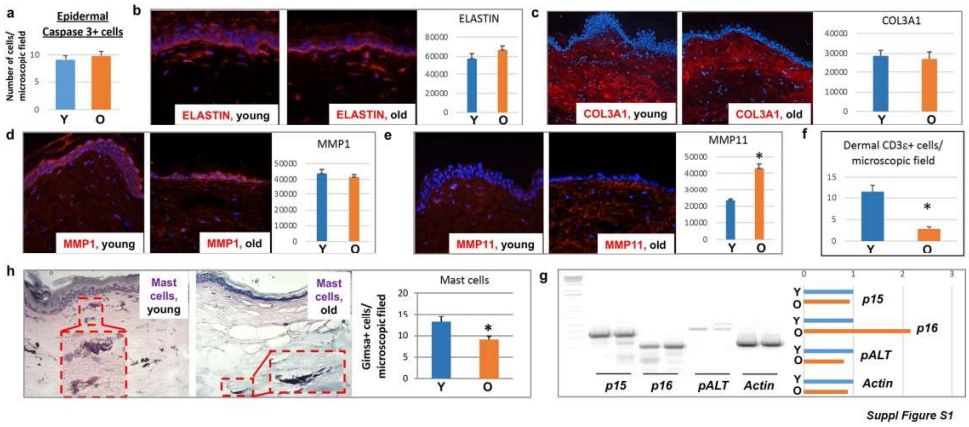

Suppl Figure S1

a

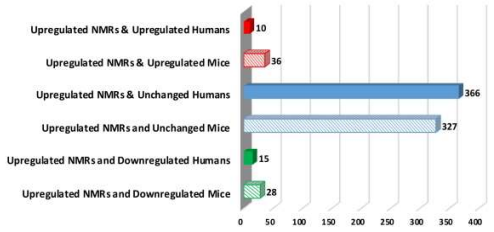
Upregulated NMRs & Upregulated Humans
10
Upregulated NMRs & Upregulated Mice
36
Upregulated NMRs & Unchanged Humans
366
Upregulated NMRs and Unchanged Mice
327
Upregulated NMRs and Downregulated Humans
15
Upregulated NMRs and Downregulated Mice
28
0 50 100 150 200 250 300 350 400

b

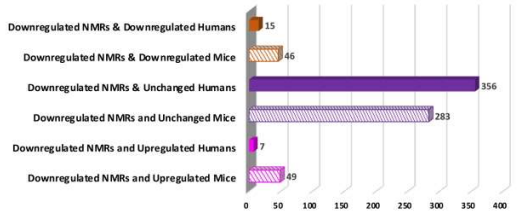
Downregulated NMRs & Downregulated Humans
15
Downregulated NMRs & Downregulated Mice
46
Downregulated NMRs & Unchanged Humans
356
Downregulated NMRs and Unchanged Mice
283
Downregulated NMRs and Upregulated Humans
7
Downregulated NMRs and Upregulated Mice
49
0 50 100 150 200 250 300 350 400

Figure S2

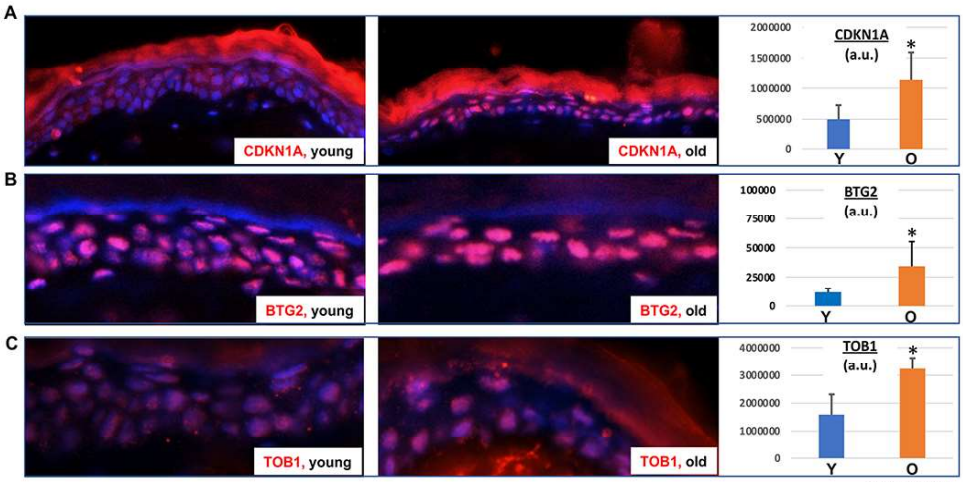

Suppl Figure S3

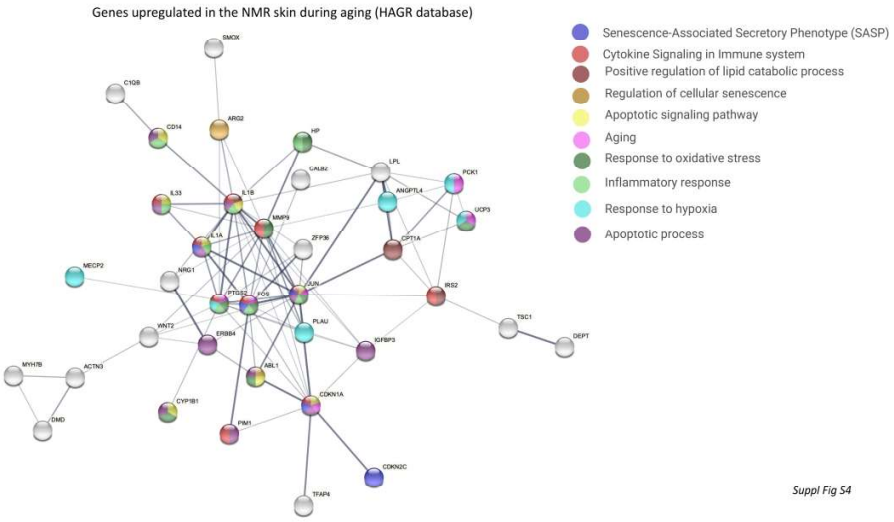
Genes upregulated in the NMR skin during aging (HAGR database)
Senescence-Associated Secretory Phenotype (SASP)
Cytokine Signaling in Immune system
Positive regulation of lipid catabolic process
Regulation of cellular senescence
Apoptotic signaling pathway
Aging
Response to oxidative stress
Inflammatory response
Response to hypoxia
Apoptotic process
SMOX
C1QB
CD14
ARG2
HP
LPL
PCK1
ANGPTL4
IL33
IL1B
MMP9
IL1A
ZFP36
CPT1A
MECP2
NRG1
IRS2
TSC1
DEPT
WNT2
ERBB4
PLAU
IGFBP3
MYH7B
ACTN3
ABL1
CYP1B1
CDKN1A
DMD
PIM1
CDKN2C
TFAP4

Suppl Fig S4

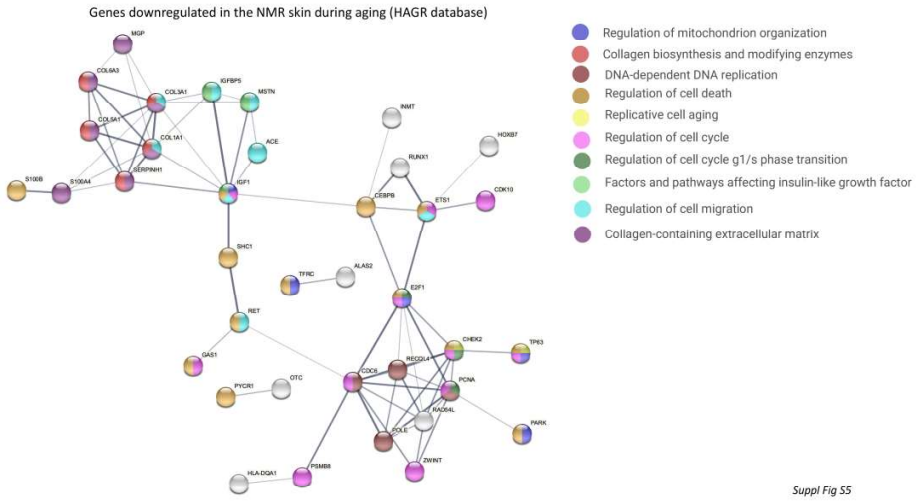
Genes downregulated in the NMR skin during aging (HAGR database)
MGP
COL6A3
COL3A1
IGFBP5
MSTN
COL5A1
COL1A1
ACE
SERPINH1
S100B
S100A4
IGF1
INMT
HOXB7
RUNX1
CEBPB
ETS1
CDK10
SHC1
TFRC
ALAS2
E2F1
RET
GAS1
CHEK2
TPE3
RECQL4
CDC6
PCNA
PYCR1
OTC
RAD54L
COL1C
PARK
ZWINT
PSMB8
HLA-DQA1
Regulation of mitochondrion organization
Collagen biosynthesis and modifying enzymes
DNA-dependent DNA replication
Regulation of cell death
Replicative cell aging
Regulation of cell cycle
Regulation of cell cycle g1/s phase transition
Factors and pathways affecting insulin-like growth factor
Regulation of cell migration
Collagen-containing extracellular matrix

Suppl Fig S5